attack. The particular effectiveness of Mg^{2+} as a template for chelate binding of ATP and ADP, bending the P—O—P link and exposing the bridging oxygen, is attributable to the cation's relatively small ionic radius and large charge-to-radius ratio. Among the cations that are present in the biological milieu in greater than trace amounts, namely, the so-called bulk metals, Na^+, K^+, Ca^{2+} and Mg^{2+}, the magnesium ion is the smallest.

We are grateful for technical help from Mr Brian Tucker (Buffalo) and Monsieur Daniel Bayeul (Nancy), and for research support from USDHHS PHS NIH grant No. GM34073. RHB is grateful for the hospitality of the Laboratoire de Cristallographie à le Université de Nancy during a three-month visiting professorship in the Spring of 1988.

References

BLESSING, R. H. (1989). *J. Appl. Cryst.* **22**, 396–397, and references cited therein.
CALVO, C. (1965). *Can. J. Chem.* **43**, 1139–1146.
CALVO, C. (1967). *Acta Cryst.* **23**, 289–295.
CROMER, D. T. & WABER, J. T. (1974). *International Tables for X-ray Crystallography*, Vol. IV, edited by J. A. IBERS & W. C. HAMILTON, Table 2.2B, pp. 99–102. Birmingham: Kynoch Press. (Present distributor Kluwer Academic Publishers, Dordrecht.)
FISCHER, R. X. (1985). *J. Appl. Cryst.* **18**, 258–262.
FRENCH, S. & WILSON, K. (1978). *Acta Cryst.* A**34**, 517–525.
GABE, E. J., LEE, F. L. & LE PAGE, Y. (1985). *Crystallographic Computing* 3, edited by G. M. SHELDRICK, C. KRÜGER & R. GODDARD, pp. 164–174. Oxford: Clarendon Press.
JOHNSON, C. K. (1970). *ORTEP*. Report ORNL-3794, 2nd revision. Oak Ridge National Laboratory, Tennessee, USA.
LUKASZEWICZ, K. (1961). *Rocz. Chem.* **35**, 31. [As cited by Calvo (1967).]
LUKASZEWICZ, K. (1967). *Bull. Acad. Pol. Sci. Ser. Chim.* **15**, 53. [As cited by Calvo (1967).]
MERRITT, E. A. & SUNDARALINGAM, M. (1980). *Acta Cryst.* B**36**, 2576–2584.
MOTHERWELL, S. (1970). *PLUTO*. Program for plotting molecular and crystal structures. Univ. of Cambridge, England.
OKA, J. & KAWAHARA, A. (1982). *Acta Cryst.* B**38**, 3–5.
ROBERTSON, B. E. & CALVO, C. (1968). *Can. J. Chem.* **46**, 605–612.
SABAT, M., CINI, R., HAROMY, T. & SUNDARALINGAM, M. (1985). *Biochemistry*, **25**, 7827–7833.
SHELDRICK, G. M. (1976). *SHELX*76. Program for crystal structure determination. Univ. of Cambridge, England.
STEWART, R. F., DAVIDSON, E. R. & SIMPSON, W. T. (1965). *J. Chem. Phys.* **42**, 3175–3181.

Acta Cryst. (1992). B**48**, 376–389

Symmetry Determination and Pb-Site Ordering Analysis for the $n = 1, 2$, $Pb_xBi_{2-x}Sr_2Ca_{n-1}Cu_nO_{4+2n+\delta}$ Compounds by Convergent-Beam and Selected-Area Electron Diffraction

BY P. GOODMAN

School of Physics, University of Melbourne, Parkville, Australia 3052

P. MILLER

Division of Materials Science and Technology, CSIRO, Locked Bag 33, *Clayton, Australia* 3188

T. J. WHITE

Electron Microscope Centre, University of Queensland, St Lucia, Queensland, Australia 4076

AND R. L. WITHERS

Research School of Chemistry, Australian National University, GPO Box 4, *Canberra, Australia* 2601

(*Received* 9 *September* 1991; *accepted* 3 *February* 1992)

Abstract

An examination of various preparations from the structural series $Pb_xBi_{2-x}Sr_2Ca_{n-1}Cu_nO_{4+2n+\delta}$ by selected-area and convergent-beam electron diffraction (SAD and CBED) shows that despite superstructural symmetries which range from monoclinic to orthorhombic, space groups *Amaa* or *A*2*aa* can be unambiguously identified for the subcells of different samples (here for $n = 1$ and $n = 2$ respectively), independently of the long-range superstructural result. An analysis of the $n = 2$ compound within the compositional range $x = 0.2 \rightarrow 0.3$ shows that both Pb-independent and Pb-dependent superlattices coexist for this range of x, the former superlattice retaining the superspace-group symmetry of

0108-7681/92/040376-14$06.00

N.A2aa.111. Following this, a semi-quantitative analysis is made using data from a commensurate Bi—Sr—Fe—O superstructural refinement. The most probable siting of Pb atoms within the Bi—O layers is determined, and a model consisting of a semi-random array of commensurate supercells derived, which accounts qualitatively for the appearances of both the observed incommensurate superlattices. A more general description of these structures requires consideration of low-angle crystallographic shear (CS) planes, identified from SAD data. Their existence may be used to explain the present variability of space group, and of superconducting properties, found for these componds over a range of cation stoichiometries and preparation procedures.

1. Introduction

The structural series $Pb_xBi_{2-x}Sr_2Ca_{n-1}Cu_nO_{4+2n+\delta}$ with $n = 1, 2, 3$ have become known as the 2201, 2212 and 2223 compounds, in conjunction with their initial discovery and subsequent study as high T_c superconductors (Maeda, Tanaka, Fukutomi & Asano, 1988). These compounds have a great deal of crystallographic interest in their own right, although investigation of the relationship between structural (*e.g.* order–disorder) and superconducting properties currently provides a major incentive for their structural refinement.

The 2212 and 2201 compounds have been the most studied of these compounds, reflecting the ease of their preparation, in contrast to that of the metastable 2223 form. One consequence of these studies is that a debate has ensued over the centrosymmetry or otherwise of the parent or subcell structures of these essentially modulated structures. This evidence is summarized in Table 1.

A second issue is that of the symmetry and nature of the superstructures associated with these compounds. So far, results obtained from electron and X-ray diffraction suggest that these consist of two incommensurate modulations, incommensurately related one to the other, one of which is associated with both the Pb-free and the Pb-doped structures, the other being associated with the Pb-bearing structures only. It is convenient to label these as type (1) and type (2) modulations, and identify them by their primary modulation wavevectors q_1 and q_2. Analyses have been made for this superstructure using four-dimensional space-group theory (de Wolff, Janssen & Janner, 1981), so far mainly for the q_1 superstructure (*e.g.* Withers, Anderson, Hyde, Thomson, Wallenberg, Fitzgerald & Stewart, 1988), and some of these results are given in Table 2. In addition, X-ray single-crystal structure refinement (Petricek, Gao, Lee & Coppens, 1990) has determined the origin of the q_1 modulation to be the incorporation of additional O atoms in the Bi—O planes of the Pb-free 2212 structure. Further to this, neutron diffraction refinement of the Pb-bearing 2212 structure (Sequeira, Rajagopal, Sastry, Yakhmi & Iyer, 1991) has shown that the Pb atoms substitute on Bi sites of this structure as Pb^{4+}. One problem here is that while X-ray diffraction data cannot be used to refine the O-atom positions, or distinguish the Pb positions in the presence of Bi, single-crystal data can be used to refine the superlattice. By contrast, neutron diffraction Rietveld analysis can address the Pb/Bi substitution problem but cannot refine the superlattice. On the other hand, a combined X-ray and neutron Rietveld analysis has been carried out on the Pb-free 2212 structure by Yamamoto (1991), which confirms the origin of the q_1 modulations as arising from a Bi—O layer distortion caused by the periodic inclusion of additional O atoms, but in which the refinement is based on the parent-structure symmetry of *Amaa* instead of the *A2aa* assumed in the Petricek refinement. From this review it is clear that the issue of the parent space group needs to be resolved independently and ahead of X-ray and neutron diffraction refinements.

At this stage it appears that electron diffraction has an important role to play as a technique which is sensitive to both space-group symmetry and superlattice geometry, and for which analytical electron microscopy (using energy-dispersive X-ray spectros-

Table 1. *Space-group results found for the* 2212 *and* 2201 *structures by the various techniques*

Technique	Space group	Reference
2212 structure		
CBED	*Amaa* or *A2aa*	Withers *et al.* (1988)
CBED	*Amaa*	Fung *et al.* (1989)
CBED, LACBED	*Amaa*	Zhang *et al.* (1990)
CBED	*A2aa*	Kan *et al.* (1990)
CBED, LACBED	*A2aa*	Present work
Neutron diffraction	*A2aa*	Bordet *et al.* (1988)
Neutron diffraction	*Amaa*	Sequeira *et al.* (1991)
X-ray diffraction	*A2aa*	Petricek *et al.* (1990)
2201 structure		
CBED	*Amaa*	Wen *et al.* (1989)
CBED	*Amaa*	Present work
X-ray diffraction	*A2aa*	Gao *et al.* (1988)

Table 2. *Symmetry of results for supergroup-symmetry determinations of* q_1 *and* q_2 *superstructure*

References	Superspace group
2212 Structure (q_1)	
Withers *et al.* (1988)	*N.Ama*.11 or *N.A2aa*.111
Yamamoto, Hirotsu, Nakamura & Nagakura (1989)	*N.Ama*.111 or *N.A2aa*.111
Petricek *et al.* (1990)	*N.A2aa*.111
Yamamoto (1991)	*N.Ama*.111
2201 Structure ($q_1 + q_2$)	
Gao *et al.* (1988)	*P.Aa*.1

copy, or EDS) can resolve Pb as a percentage in the presence of Bi.

In the present work, we have made use of the availability of material in both micaceous single crystal and granular form, to carry out convergent-beam and 'large-angle' convergent-beam electron diffraction (CBED and LACBED), for which extended single-crystal surfaces normal to the long axis are required (§3), and three-dimensional characterization of the superlattice by selected-area diffraction (SAD), for which equal access to all orientations (provided by an ion-beam-thinned polygranular sample) is required (§4). In both these investigations EDS analysis is available.

2. Preparation and initial electron diffraction characterization

Single crystals of the 2212 phase were grown by the CuO flux method in alumina crucibles by the following procedure: PbO, Bi_2O_3, $SrCO_3$, $CaCO_3$ and CuO were mixed in proportions 0.25:1.75:1.5:2.0:4.5 with respect to the cation ratios. After calcining at 1073 K the mixture was re-ground and heated gradually to 1298 K. The melt was held for 16 h, then held successively at 1193 and 1123 K for equivalent periods, using streaming oxygen at the lower temperature, before finally cooling slowly to room temperature.

In order to form single crystals of the 2201 structure, additional PbO was added to the starting mixture of give the Pb:Bi ratio of 0.35:1.65.

Single crystals were extracted from these preparations by cutting sections through the alumina crucibles with a diamond saw, and examining these sections under a binocular microscope. Individual sheet crystals were selected, and subsequently glued to a 50-mesh copper grid. Transmission electron microscope single-crystal thin-film samples were then prepared by cleaving these to transparency.

Crystals of the 2212 and 2201 preparations were found to have compositions $Pb_{0.16}Bi_{1.84}Sr_{2.2}Ca_{0.8}Cu_{(2)}O_y$ and $Pb_{0.2}Bi_{1.8}Sr_{1.9}Ca_{0.4}Cu_{(1)}O_y$ respectively, as determined by EDS, where Cu was not measured since the specimen was on a Cu grid, and where the Sr/Bi ratio is the least-reliable measurement.

Single-crystal growth by the above method could not be induced to yield high-Pb crystals of the 2212 form; instead initial high-Pb proportions led to 2201 as a single phase. Sintered 2212 material with a higher Pb content was however obtained starting from a solution rather than dry materials. Thus by rapid evaporation of a nitrate solution in 50% nitric acid, with the metals Pb:Bi:Sr:Ca:Cu in the ratio 0.2:0.8:0.8:1.0:1.4, the components could be obtained in a finely divided and reactive state. Following a low-temperature decomposition of the nitrates, the resulting oxide mixture was pelletized and fired in an alumina boat for 4 days in a monitored mixture of pure nitrogen and air at 1105 K, followed by slow cooling in oxygen. The final composition determined by EDS was $Pb_{0.23}Bi_{1.77}Sr_{1.7}Ca_{1.3}Cu_2O_y$. Polygranular samples from this sinter were prepared for electron microscopy by mechanical dimpling, followed by ion-beam milling to transparency using a liquid-nitrogen-cooled holder to prevent crystalline melting.

Single crystals of the Pb-free 2212 material suitable for cleavage preparation as extended thin-film samples were obtained from another laboratory.

2.1. *Initial electron diffraction characterization*

Fig. 1 shows the [001] SAD zone-axis patterns obtained from the above samples. As can be seen in this comparative series, the symmetry and intensity modulation of the satellite reflections varies with both composition and structure.

Fig. 1(*a*) shows that for the Pb-free crystal of 2212 composition, the satellite rows run obliquely through the sublattice rows parallel to a^*. The same effect has been reported by Kan, Kulik, Chow & Moss (1990) for this compound. This means, as recorded by these authors, that the modulation wavevector in this case has a b-axis component, so that $q_1 = c^* + \gamma_1 a^* + \delta_1 b^*$ breaking the orthorhombic symmetry and modulation vector $q_1 = c^* + \gamma_1 a^*$ assumed by the authors listed in Table 2, for the 2212 compound.

Fig. 1(*b*) shows the similar [001] pattern from the cleaved single-crystal film crystal of the 2212 structure with a Pb/Bi substitution in the ratio 1/12. The main difference observable from the pattern of Fig. 1(*a*) is the collinearity of the satellite rows, so that the simpler orthorhombic form of q_1 appears valid.

Fig. 1(*c*) shows the pattern from the sintered 2212 compound, with lead substitution of $1/7 > Pb/Bi > 1/8$, characterized by a set of strong superlattice orders and strong thermal-diffuse scattering near the central beam. As with Fig. 1(*b*) the superlattice rows appear strictly collinear, the most obvious difference here being the greater strength of higher-order satellite reflections between the main Bragg reflections. An additional Pb-induced superlattice with the primary wavevector q_2 is evident in regions close to the main Bragg spots, particularly in regions of the pattern away from the central region.

Fig. 1(*d*) shows the [001] pattern from the 2201 extended single-crystal sample of the 2201 structure with $Pb/Bi \simeq 1/9$, Here the satellite reflections are uniformly strong and collinear between the main reflections, although they are not as regularly spaced as those appearing in Fig. 1(*c*).

All these patterns have in common a certain quasi-periodic component *i.e.* in patterns like those of Figs.

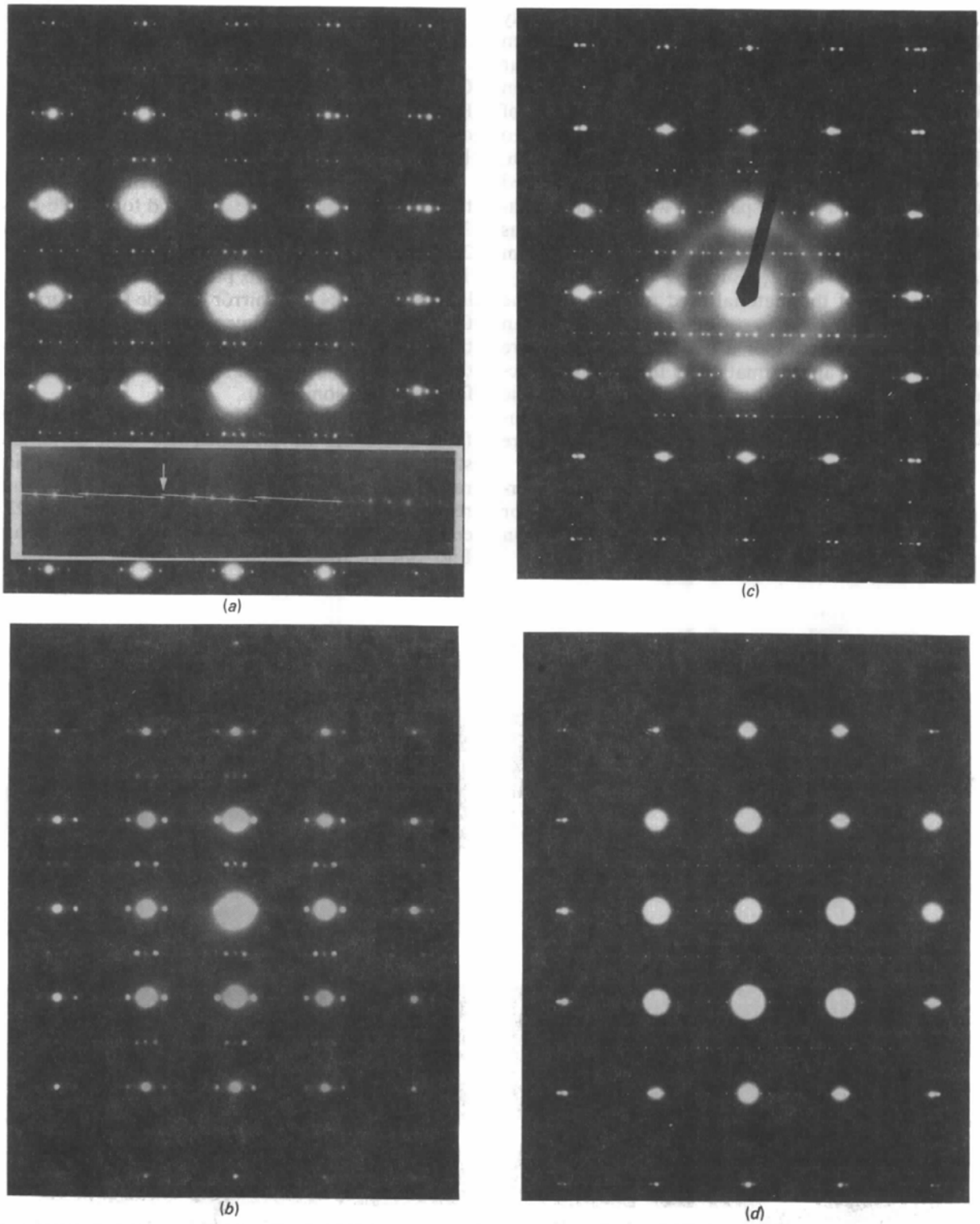

Fig. 1. [001] selected-area zone-axis patterns from the various compounds of the $Pb_xBi_{2-x}Sr_2Ca_{n-1}Cu_nO_{4+2n+\delta}$ form. (*a*) Pattern from the Pb-free 2212 structure (cleaved crystal sample). Insert shows an enlarged section of a satellite row running between the main Bragg spots ($k = 2n + 1$), showing that the row is composed of sloping line segments. An arrow indicates a region where the gap between segments can be observed. (*b*) Similar pattern from cleaved crystal film with a Pb/Bi substitution of approximately 1/12. (*c*) [001] pattern from sintered 2212 material with Pb/Bi substitution $\sim 1/7$, showing strong $\langle 110 \rangle$ directed diffuse streaking. (*d*) [001] pattern from a cleaved single crystal of the 2201 structure (with the beam focussed on the photographic plate).

1(*c*) and 1(*d*) the satellite reflections, most notably those along the $k = 2n + 1$ rows (the rows between main Bragg spots), are not spaced at strictly regular intervals. The origin of this irregularity can be seen from Fig. 1(*a*) where individual line segments of diffraction are resolved, with a slight inclination to the b^* direction. When, with another composition, collinearity is restored to the b^* row, this segmented nature is retained in the spacings, which reflect separate origins for each segment. This phenomenon has been documented as 'swinging shear planes', from earlier studies of TiO_{2-x} (Bursill & Hyde, 1972).

In the case of the material used for Fig. 1(*c*), the spacings are very close to periodic, indicating that an interpretation in terms of a periodic superstructure will give a good approximation to the average structure, though in the final analysis the quasi-periodic nature requires the interpretation of a finer non-periodic microstructure. These stages of analysis are followed in §4 and §5 below.

Almost independently from these details, the average space group deriving from the basic subcell or parent structure can be determined by CBED as in the following section.

3. Three-dimensional space-group determinations using CBED and LACBED

CBED and LACBED patterns were obtained using a Philips CM30 microscope fitted with a Gatan double-tilt liquid-nitrogen-cooled stage operating at 103 K.

Central beam (bright-field) LACBED patterns for the Pb-doped and Pb-free 2212 and for the Pb-doped 2201 compound are shown in Figs. 2(*a*), 2(*b*) and 2(*c*) respectively. All three cases show *mm* symmetry. These patterns fulfil two purposes. First they establish the existence of a mirror or glide plane normal to the projection, hence permitting allocation of a three-dimensional space group. Second it follows that the area under examination is free from stacking faulting (Johnson, 1972).

In view of the possible controversy of stacking-fault detection in an otherwise centrosymmetric structure raised by Zhang, Yan & Fung (1990) in a report we received after our analysis, we should re-examine the LACBED patterns from the 2212 compound for accuracy as follows: the pattern of Fig. 2(*a*) for the Pb-doped specimen comes from an

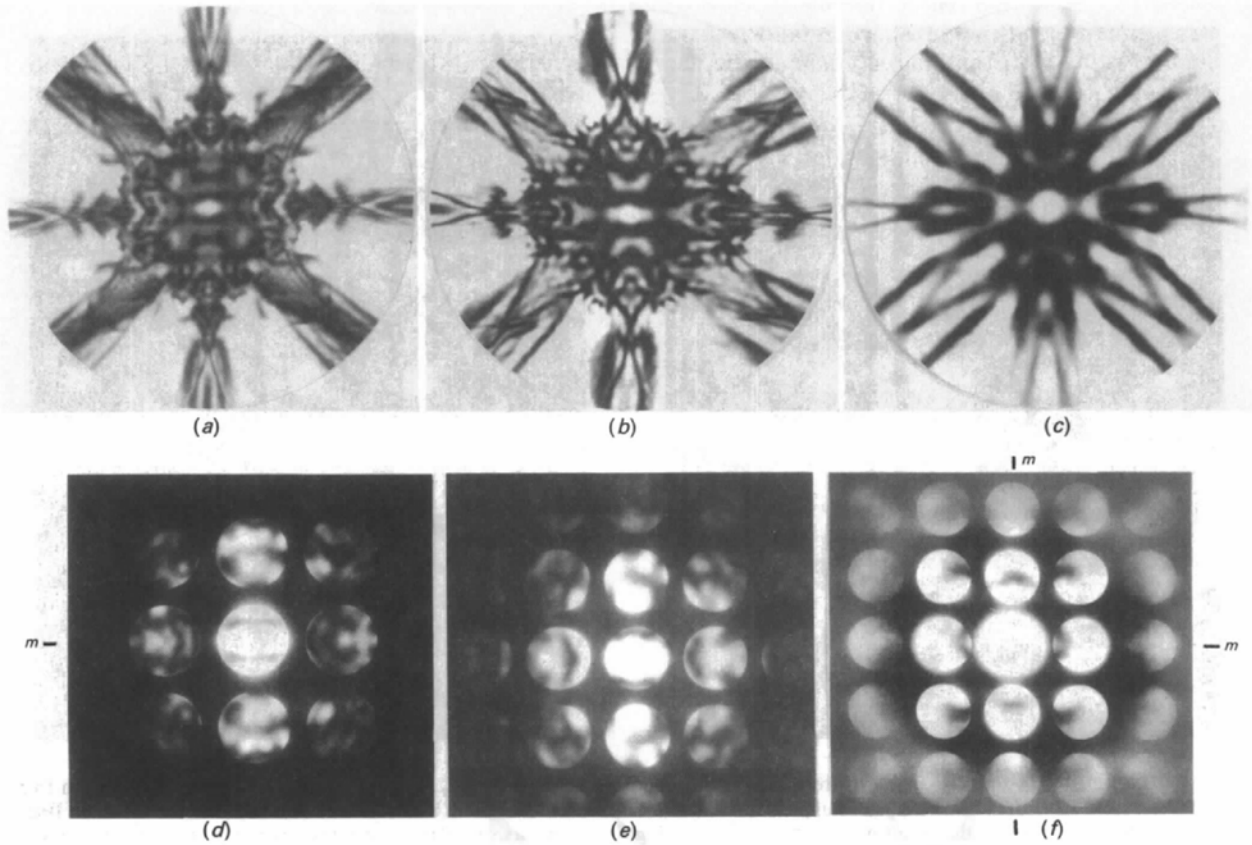

Fig. 2. Bright-field [001] LACBED patterns for $Pb_xBi_{2-x}Sr_2Ca_{n-1}Cu_nO_{4+2n+\delta}$: (*a*) for polytype $n = 2$, $x = 0.16$; (*b*) for polytype $n = 2$, $x = 0$; (*c*) for polytype $n = 1$, $x = 0.10$. (*d*), (*e*), (*f*): CBED patterns (central region) for the same samples. All patterns have a mirror line indicated by the horizontal mark *m*–*m*; only (*f*) has the second mirror line.

almost ideally flat region and is accurately *2mm*; that from the Pb-free sample in Fig. 2(*b*) is less perfect. Therefore our strongest conclusions relate to the former sample.

The corresponding zero-layer CBED patterns for the three samples are shown in Figs. 2(*d*)–2(*f*), while more complete patterns from which the *c* axis was determined are shown in Figs. 3(*a*) and 3(*b*). The CBED patterns from both Pb-free and Pb-bearing 2212 compounds exhibit *1m* symmetry both in zero and upper-layer patterns (Figs. 2*d* and 4*a*), implying a three-dimensional point-group symmetry (considering the LACBED result) of *2mm*, while the corresponding patterns from the 2201 compound exhibit *mm* symmetry, implying a three-dimensional point-group symmetry *mmm*.

Finally, the pair of dark-field LACBED distributions for the 220 and 220 beams from the $n = 1$ specimen are shown in Figs. 4(*a*) and 4(*b*). These intensity distributions are virtually identical in all details, giving a more accurate proof of centrosymmetry than that given by Fig. 2(*c*). The sensitivity of this extension of the $+G/-G$ test (Tanaka, Terauchi & Kaneyama, 1988; Goodman, 1975) arises from the fact that both patterns are taken from the same crystal area and therefore both the real-space and (if centrosymmetric) diffraction-space detail are identical. Contrasting with this, Fig. 4(*c*) shows the dark-field 020 intensity distribution from the same region, in which a lack of perfection of the central mirror line (from the rotation diad of the space group) arises from real-space crystal distortion (crystal curvature).

The above observations demonstrate that the lower symmetry of *A2aa* holds for all the compositions of the 2212 structure which we have examined, (including those with 12% Pb substitution taken from a sintered material and not shown here), and that the 2201 sample alone has the higher symmetry of *Amaa*.

One observation to be made from these findings is that the CBED-determined symmetry appears to be independent of the superlattice symmetry and dependent upon the average sublattice structure. This is consistent with our understanding firstly of scattering theory which would suggest that an incommensurate lattice would not in first order interact dynamically with the base lattice except through the central beam. This has the effect of decoupling the symmetries of the two (sub- and super-) lattices which should be separately displayed in the CBED pattern. [This effect has been confirmed for example by Tanaka *et al.* (1988) in observations on $Sr_2Nb_2O_7$.] Secondly, this can be understood from the relative weakness of the superlattice reflections in the vicinity of the main zero-layer (ZOLZ) reflections

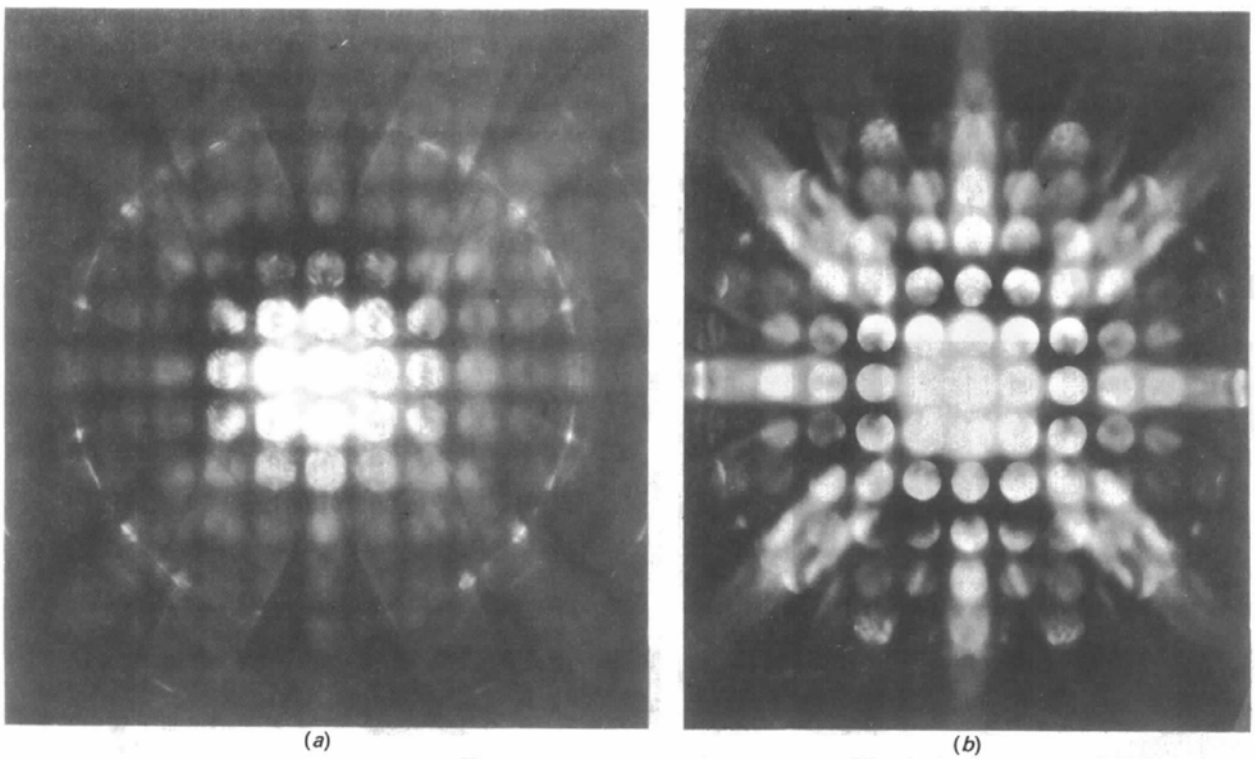

(*a*) (*b*)

Fig. 3. The [001] CBED patterns taken with a smaller camera length to show the first-order Laue zone (FOLZ) lines from which the *c* axis was measured. (*a*) $n = 2$ polytype. (*b*) $n = 1$ polytype.

used in the CBED analysis. Experimentally it is found that the superlattice reflections only contribute to the main CBED reflections at higher $\sin(\theta/\lambda)$ values and that the inner reflection discs have no detectable superlattice contribution.

Hence as expected the CBED/LACBED results give a space group strictly relevant to the sublattice or parent structure in each case. This is the space group, however, which appears to be an initial requirement in neutron diffraction Rietveld refinements.

Table 1 lists comparative findings from electron, neutron and X-ray diffraction for the two structures under discussion. Regarding other electron diffraction results, we are in agreement with Wen, Liu, Ren, Yan, Zhou & Fung (1989) with respect to the 2201 structure and with Kan *et al.* (1990) with respect to the 2212 structure, but in disagreement with Fung, Yang & Yan (1989) who found *Amaa* for the 2212 structure [repeated in the later publication of Zhang *et al.* (1990)].

3.1. *Conclusions*

Initially, it is necessary to determine whether the variability of results displayed in Table 1 arises from an experimental indeterminacy for a marginally non-centrosymmetric structure, or from the existence of two distinct atomic arrangements. Our present results give convincing evidence that the latter explanation is correct. What emerges from these and other results is that two stable orthorhombic space-group symmetries exist for both 2201 and 2212 structures, although one clear result (centro- or non-centrosymmetry) will be found for any particular preparation. Discussion of possible origins for this symmetry switching will be left until §5.

4. Superlattice analysis of sintered 1/7 Pb/Bi 2212 material from an incommensurate basis

The superlattice reflections have hitherto been analysed largely on the basis of a true incommensurate superstructure. This is because the diffraction patterns from both electron and X-ray diffraction index in first approximation in this manner, as noted above, even though, when examined in closer detail, there are signs in the electron diffraction data (namely differences in diffuse peak widths and irregularities in diffraction spacings) that indicate this interpretation is the result of taking an averaged structural view. Notwithstanding this objection, the determination of a superspace group is useful, both to allow comparison with previous results of the same determination, and to provide a basis for such averaged structural refinements as neutron and possibly X-ray diffraction analyses.

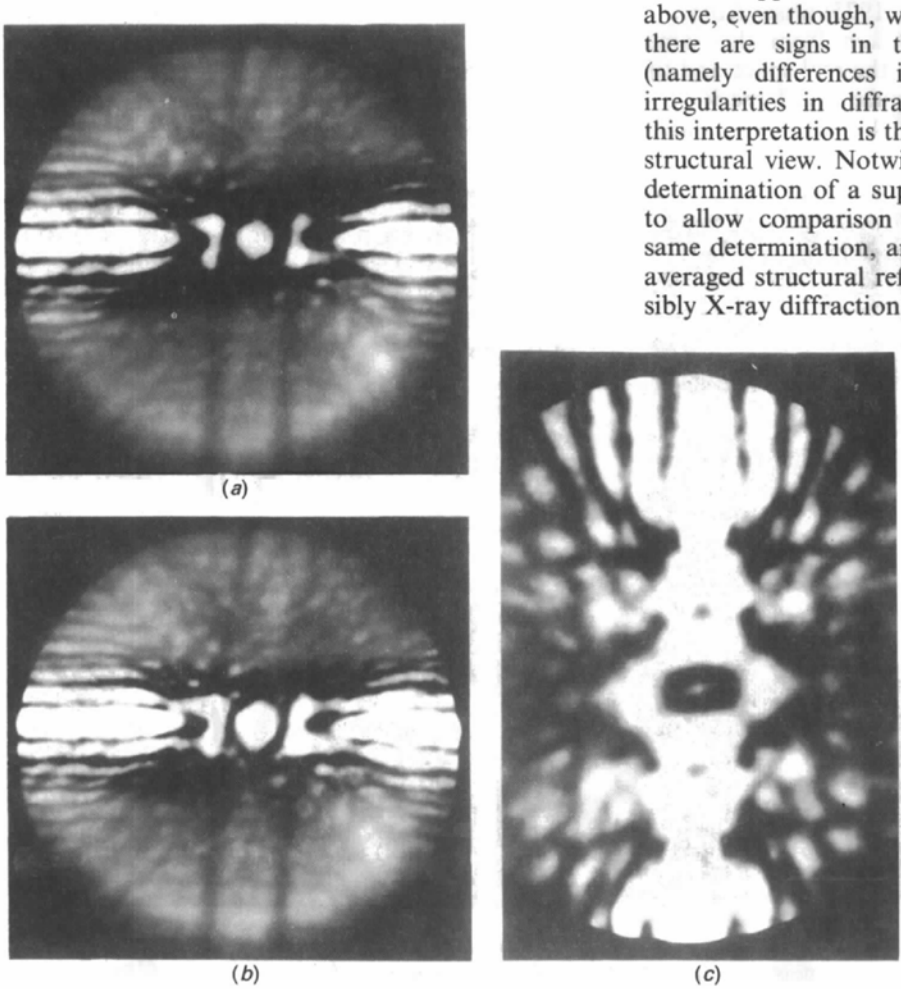

Fig. 4. Dark-field LACBED patterns from the $n = 1$ material near [001]. (*a*) and (*b*) 220 and $\bar{2}\bar{2}0$ patterns; (*c*) 020 pattern.

The 2212 material with an approximate 1/7 ratio for Pb/Bi was chosen for superlattice analysis because it gives strong diffraction from the two types of superlattice, with a close approach to regularity in the diffraction pattern. This preparation was examined on both a JEOL 100 CX electron microscope and a Philips CM30 microscope, both fitted with side-entry specimen stages. Three zones axes were analysed as described below.

4.1. [010] *zone*

Fig. 5 shows the [010] zone-axis pattern of the above sample. This pattern is of a type first reported by Ramesh, van Tenderloo, Thomas, Green & Luo (1988) for the Pb-bearing 2212 structure (mistakenly taken then for the 2223 structure), who also gave the interpretation in terms of a newly discovered Pb-dependent superlattice. Chen, Werder, Espinosa & Cooper (1989) later identified the two modulations correctly in the Pb-free and Pb-rich 2212 structure, and suggested the nomenclature q_1 and q_2 for the corresponding primary wavevectors.

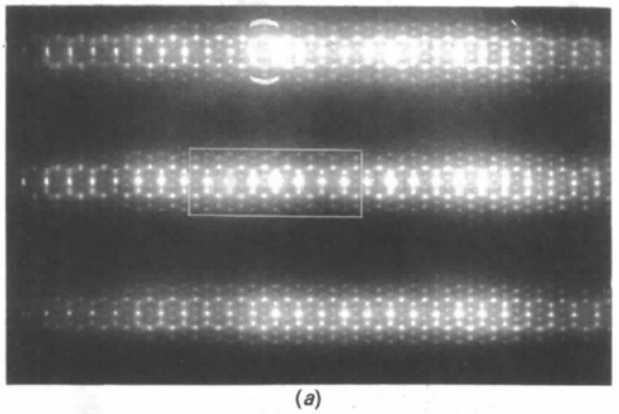

(*a*)

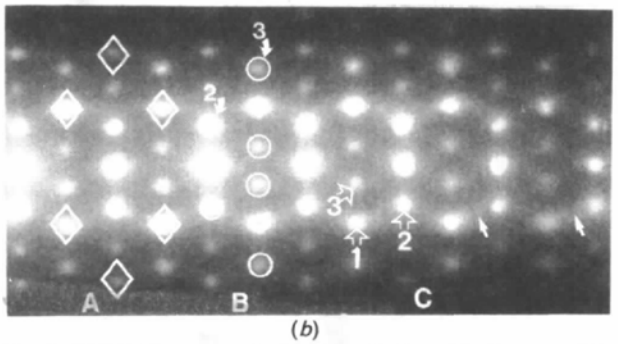

(*b*)

Fig. 5. [010] SAD patterns for $Pb_xBi_{2-x}Sr_2Ca_{n-1}Cu_nO_{4+2n+\delta}$ with $n = 2$, $x = 0.23$. (*a*) Three rows of the pattern, showing boxed central region [enlarged in (*b*)], and bracketed region on the top row, where streaking connecting the two types of superlattice is strong. (*b*) Enlarged row from (*a*), where section *A* shows a centered 'q_1' cell lattice with hexagonal boxes [type (1) satellite], section *B* shows the additional 'q_2' satellites (encircled) of types (2) and (3), and section *C* shows type (1), (2) and (3) spots, with arrows indicating diffuse streaks.

These q_1 and q_2 components are indicated in Fig. 5(*b*) by diamonds and circles respectively. Thus it can be seen that the q_1 pattern marked in section *A* of the figure has a centred geometry in [001], in accordance with superspace reflection rules given below. The remaining pattern shown as encircled reflections in section *B* of the figure and generated by the q_2 vector, has two components. The first, labelled as '2' in the figure, represents the simple type (II) superlattice as it occurs in Pb-rich samples *i.e.* a convolution around the main Bragg peaks for $L = 2n$. The second component, labelled '3' in the figure, represents a convolution of the q_2 structure around q_1 satellites.

The simplest explanation for this type (3) component would be secondary scattering, where diffraction from q_1 domains again diffracts from q_2 domains. However, the modulation of the satellite intensities with excitation error shows this to be incorrect *i.e.* the outer type (3) spots are much weaker at moderate excitation error than the corresponding inner spots, indicating that this diffraction pair has a genuine kinematic structure factor, and arises from the multiplication within the real-space structure of the two modulations. Hence the whole q_2-derived pattern becomes impossible to relate to a four-dimensional ($HKL\eta$) superspace.

Finally, strong diffuse scattering may be observed connecting the q_1 and q_2 satellite sets, indicated by arrows in section *C* of Fig. 5(*b*), and becoming even more dominant in outer sections of the pattern (indicated in upper regions of Fig. 5*a*). This streaking provides the strongest SAD evidence that a real-space interaction exists between the two modulations, and that these structures exist in the same structural layers.

4.2. *Superspace descriptions*

Assuming a parent space group of *A*2*aa*, the q_1 pattern may be indexed in the superspace group *N*.*A*2*aa*.111 (or 37*b*.14.1; de Wolff *et al.*, 1981). Using a lattice vector $g = ha^* + kb^* + lc^* + mq_1$, $q_1 = c^* + \gamma_1 a^*$ is incorporated as the new primitive translation. The notation is improved by the uppercase notation (de Wolff *et al.*, 1981), where $L = 1 + m$, and $H = h$, $K = k$, so that $Q_1 = \gamma_1 a^*$, $G = Ha^* + Kb^* + Lc^* + mQ_1$, retaining an orthogonal lattice basis and giving general conditions $K + L + m = 2n$, and $H0Lm$: $H = 2n$, $L + m = 2n$.

Only part of the $q_2 = \gamma_2 a^*$ satellite structure [the part which occurs in the absence of q_1 satellites illustrated as type (2) spots in Fig. 5(*b*)] can then be accommodated in the superspace group *P*.*A*2*aa*.111 (37*b*.13.111) ($K + L = 2n$, no further conditions).This description could still hold some analytical value if the two modulations occurred in separate parts of

the structure. Otherwise convolution of the two symmetries *N.A2aa*.111 and *P.A2aa*.111 leads to a necessary five-dimensional superspace description.

4.3. [001] *zone*

Evidence from the [001] zone axis is critical in distinguishing more subtle features of these structures, as shown by the wide differences seen for different preparations in Fig. 1. This additional sensitivity can be used to test the above superspace description, by examining enlargements from the pattern of Fig. 1(*c*), given in Fig. 6. Thus, Figs. 6(*a*), 6(*b*) and 6(*c*) show enlargements from ZOLZ, FOLZ and SOLZ (second-order Laue zone) respectively. Most of the satellite reflections seen in the ZOLZ are higher orders of the $Q_1 = 0.21a^*$ vector (using now upper-case notation throughout for consistency). In Fig. 6(*a*), higher orders of Q_1 are indexed with four-dimensional indices (*HKLm*), distinguishing them from the sublattice reflections which are indexed with three (*hkl*) indices, and from the orders of Q_2 indexed with five (*HKLmη*) indices. Thus, along the $K = 2n + 1$ central row, the first-, third- and fifth-order Q_1 satellites of the 010 parent are indexed as 0101, 0103 and 0105, while those of the 210 parent are indexed as 2101, 2103 and 2105, the two fifth-order reflections crossing the central 110 point. Along the $K = 2n$ (bottom row), second- and fourth-order Q_1 satellites 0202, 0204, appear. Reflections along both rows are consistent with the general condition $K + L + m = 2n$, and the additional condition $H = 2n$ for *HK*0 reflections, as required for the space group *N.A2aa*.111.

Observations from Fig. 7 (for the exact zone orientation), and from Fig. 6(*b*) (showing FOLZ reflections) are consistent with these conditions. Thus, the satellites 020 ± 2 and 020 ± 4, 061 ± 1 and 081 ± 1, 601 ± 1 and 621 ± 1, appear in Figs. 7(*a*), 7(*b*) and 6(*b*) respectively.

Within the ZOLZ pattern of Fig. 6(*a*), Q_2 satellite reflections appear only along the $K = 2n$ rows, as 20001, 20002 and 02001, 02002. However the first-order $\pm Q_2$ reflections, are always diffuse, and only satellites corresponding to $\pm 2Q_2$ yield sharp reflections. This is seen in Fig. 7(*c*), where only $020 \pm 2Q_2$ and $040 \pm 2Q_2$ are sharp, and in the alternative (exact zone) patterns of Figs. 7(*a*) and 7(*b*). These observations indicate that the $2Q_2$ vector, corresponding to $a_2 \simeq 3.5a$, or $7 \times a/2$, is significant in the modulation structure in this projection.

Further restrictions on the appearance of Q_2 satellites are seen in Fig. 7. This while 020 has $\pm 2Q_2$ satellites, these are absent for most of the b^* row. In particular while there are no direct Q_1 or Q_2 satellites

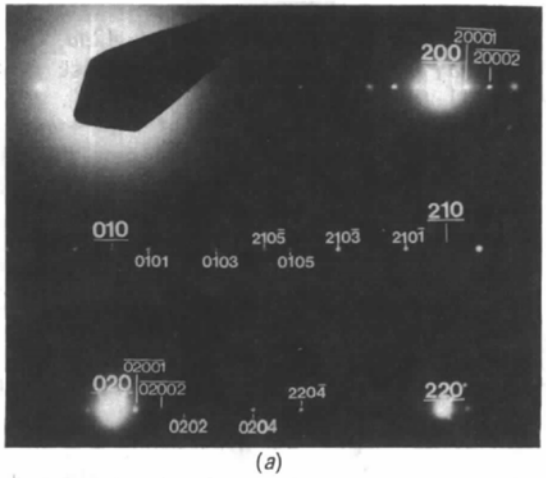

(*a*)

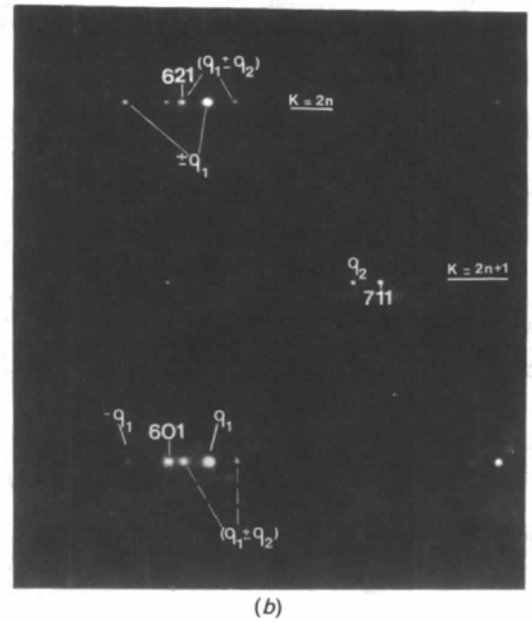

(*b*)

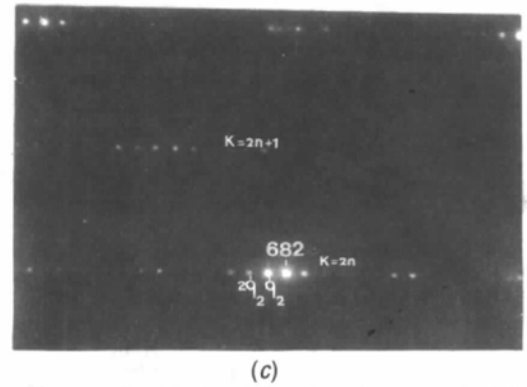

(*c*)

Fig. 6. Enlarged sections from the [001] SAD pattern of Fig. 1(*c*), taken with approximately 1° rotation from the zone orientation. (*a*) ZOLZ region: three-index, four-index and five-index notations are used to distinguish subcell, q_1 supercell and q_2 supercell reflection indices respectively. (*b*) FOLZ region, showing distribution of q_1 and q_2 satellite reflections. (*c*) SOLZ region of the same pattern.

with the 081 reflection, the difference satellite $Q_1 - Q_2$ is strong. This observation confirms the interdependence of the two modulations within the real structure, as expressed earlier *i.e.* this could not arise from external double diffraction.

4.4. [100] *zone*

The [100] zone SAD (Fig. 8) contains no satellite reflections in the ZOLZ, but confirms the *A*-centering rule $K + L = 2n$. The main FOLZ appears with reflections such as (0 0 38 0 1) and (0 1 39 0 1), corresponding to a zone spacing of $\sim 0.15a^*$ or ~ 38 Å (*i.e.* $7 \times a$). Also there is a region between zones corresponding to ~ 70 Å, the FOLZ spacing for the $Q_1 - Q_2$ spacing of $\sim 0.09a^*$ discussed above, where additional reflections such as $(00271\bar{1})$ appear.

4.5. *Conclusions*

The above analysis shows that the Q_1 superlattice follows the symmetry of supergroup *N.A2aa*.111 in three-dimensional analysis, while the appearance of Q_2 and $(Q_1 + Q_2)$ superlattice reflections do not follow space-group extinction rules and must be governed by structural details.

5. Superlattice analysis of sintered 1/7 Pb/Bi 2212 material from a commensurate basis

Further analysis in terms of a commensurate substructure is made feasible by the existence of refinement data on an analogue compound which forms a simple commensurate superlattice. The ferrite structure $Bi_{10}Sr_{15}Fe_{10}O_{46}$ characterized by a commensurate $A = 5a$ superstructure has been refined in detail by Le Page, McKinnon, Tarascon & Barboux, (1989). These authors show that the compound is 'isostructural' with the 80 K superconductor $Bi_2Sr_2CaCu_2O_{8.2}$ with respect to the development of a superstructure around the Bi—O layers. The two structures have different space groups which are related in an interesting way. The four-dimensional space group *N.A2aa*.111 projects down the *a* axis as *I*222, of which *B*222, the space group of $Bi_{10}Sr_{15}Fe_{10}O_{46}$, is a (minimal isomorphic) supergroup in the terminology of *International Tables for X-ray Crystallography* (1987, Vol. A). The extinction rules for the space groups *N.A2aa*.111, *P.A2aa*.111 and *B*222 are listed in Table 3. From this it is seen that the main difference between *B*222 and *N.A2aa*.111 in representing the q_1-modulated superconductor structure appears at the [001] orientation, where there is additional centering for *N.A2aa*.111. However, our procedure is to model in two dimensions for a single Bi—O layer, and to leave integration of this within the correct space group until a later stage.

In the following determination of Pb siting, the simplifying assumptions made are that (*a*) all the Pb atoms substitute for Bi within the Bi—O layers and

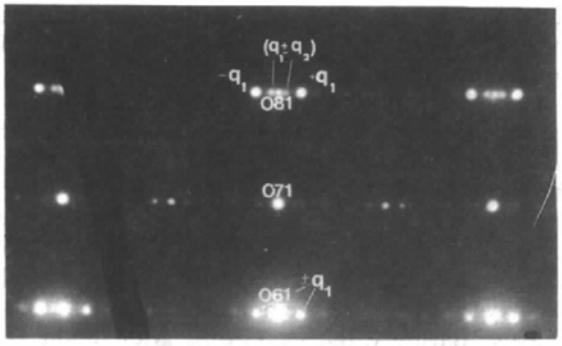

(*b*)

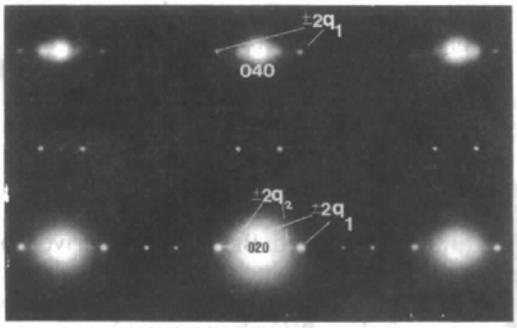

(*a*)

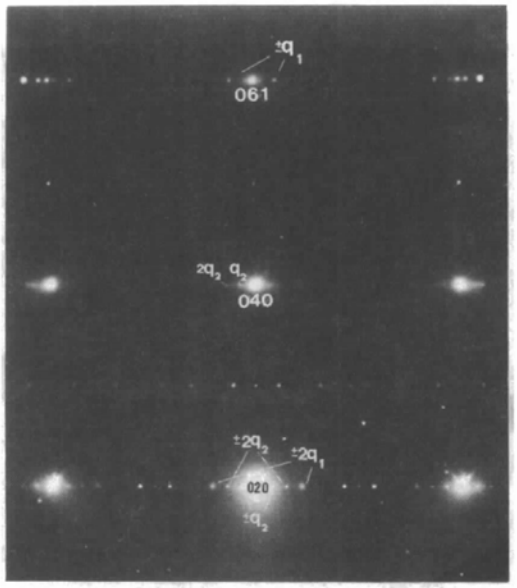

(*c*)

Fig. 7. Enlargements from the [001] pattern showing the extinction behaviour of the q_1 and q_2 satellites along the 0*kl* row. (*a*) and (*b*) Regions of 0*k*0 and 0*k*1 respectively for exact zone orientation. (*c*) 0*k*0 and 0*k*1 for approximately 1° rotation from exact zone.

Table 3. *Comparative listing of extinction rules for the space groups N.A2aa.*111, *P.A2aa.*111 *and B*222

The indices (*mKL*) and (*HKL*) are substituted alternatively for (*hkl*) in the *B*222 column for ease of comparison with the first two groups.

	*N.A2aa.*111	*P.A2aa.*111	*B*222
General	$K+L+m=2n$	$K+L=2n$	$L+m=2n;\ L+H=2n$
[011]	$L+m=2n,\ H=2n$	$L=2n,\ H=2n$	$L+m=2n;\ L+H=2n$
[001]	$K+m=2n,\ H=2n$	$K=2n,\ H=2n$	$m=2n;\ H=2n$
		Special position 4(*c*): $H+K=2n$	

Table 4. *Valence-bond sum results for the* Bi^{3+}, Pb^{2+} *and* Pb^{4+} *ions used to determine the likely* Pb*-substitution siting in the* Bi—O *chain*

Polyhedron	Bond lengths (Å)	Valence sum ($A = Bi^{3+}$, Pb^{2+}, Pb^{4+}) Bi^{3+}	Pb^{2+}	Pb^{4+}
A(1)—O_δ	1.90–3.61	3.72	3.23	3.24
A(2)—O_δ	2.07–3.43	2.71	2.84	2.35
A(3)—O_δ	2.03–3.12	2.56	2.69	2.23
A(4)—O_δ	1.80–3.68	3.56	3.74	3.10
A(5)—O_δ	2.04–3.41	2.62	2.75	2.27
		Average = 3.03		

(*b*) that charge balance is maintained locally within the Bi—O layers, by the substitution of Pb^{2+} and Pb^{4+} ions in equal numbers for Bi^{3+}. The first assumption is supported by neutron diffraction evidence (Sequeira *et al.*, 1991). Then, although no single measurement of the valence state of Pb in this compound has been reported, the existence of both Pb^{2+} and Pb^{4+} has been deduced separately in micro-Raman scattering and neutron profile refinement analysis respectively (Boekholt, Götz, Idink, Fleuster, Hahn, Woermann & Guntherodt, 1991; Sequeira *et al.*, 1991). It therefore seems quite reasonable to assume that both species are substituted in some semi-ordered way in order to maintain charge balance. The level of Pb incorporation is then set by the micro-analytical determination of the Pb/Bi atomic ratio as: $1/8 > Pb/Bi > 1/7$. The topology of a Bi—O layer in $Bi_{10}Sr_{15}Fe_{10}O_{46} \equiv Bi_2Sr_3Fe_2O_{9+\delta}$ ($\delta = 0.2$) is shown in Fig. 9(*a*), emphasizing the incorporation of an additional O atom between the Bi(1) positions brought about by a change in local bonding. This in turn introduces a variability in Bi—O distances along the whole Bi—O chains. If Pb substitution in this structure is to occur with a charge balance, Pb incorporation must be accompanied either by oxygen intercalation ($Bi^{3+}Bi^{3+}\blacksquare \rightarrow Pb^{4+}Pb^{4+}O^{2-}$) or the creation of oxygen vacancies ($Bi^{3+}Bi^{3+}O^{2-} \rightarrow Pb^{2+}Pb^{2+}\blacksquare$). The bond-valence sums for Bi in $Bi_{10}Sr_{15}Fe_{10}O_{46}$ are summarized in Table 4. Individually all Bi atoms are significantly under- or overbonded, although the average valence is close to 3. The oxygen ions similarly show wide variation in valence. Since the topology of the Bi—O layers will be equivalent in the cuprate, an estimate of the most likely siting of Pb can be made on the basis of bond-valence summing. Without relaxation of the oxygen bonds or the addition or subtraction of oxygen, Pb^{4+} and Pb^{2+} are invariably under- and overbonded respectively. However, it is apparent from the [001] projection (Fig. 9*a*) that an additional equatorial oxygen may be placed between the Bi(1) sites, raising their coordination to 7. The bond-valence sum for Pb^{4+} in this site is raised to ~4.4 (3.2 + 1.2) which is a little high, but could be reduced to nearer 4 by slight relaxation of the PbO_7 polyhedron. Accordingly, the Bi(1) site is considered the most likely location for Pb^{4+}. In the case of divalent Pb, whose incorporation requires the removal of oxygen, the most probable site is Bi(4), which is significantly overbonded (3.74). Removal of one oxygen ['O(4)', in the nomenclature of Tarascon, Le Page, Barboux, Bagley, Greene, McKinnon, Hull, Giroud & Hwang (1988)], would significantly reduce the bond-valence sum for this site and result in a PbO_5 polyhedron. Therefore, we conclude that Bi(4) is the most likely position of Pb^{2+}. Although PbO_2 and PbO_5 valence sums might normally be considered outside the acceptable range, it should be remarked that BiO_6 sums in the unsubstituted refined ferrite structure are also variable.

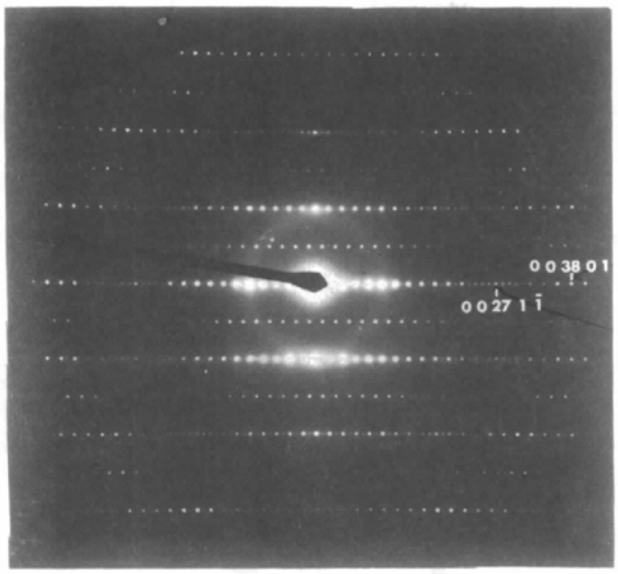

Fig. 8. [100] Selected-area diffraction pattern from the same sample used for Fig. 1(*c*).

The result of this analysis is shown in Fig. 9. Fig. 9(*a*) shows the undoped Bi—O layer derived by Le Page *et al.* (1989) in which the additional bridging oxygen sites are shown, together with the numbering of Bi sites 1–5. Fig. 9(*b*) shows a replacement of all Bi(1) and Bi(4) sites with partial occupation, while Fig. 9(*c*) shows an individual result with one each of

Bi(1) and Bi(4) replaced with Pb^{4+} and Pb^{2+} with the required spacing of $3.5 \times a$ (giving a repeat of $7 \times a$ overall).

5.1. *Derivation of the incommensurate superstructures*

Using the above model (Figs. 9*b* and 9*c*), we find that the simplest arrangement which will give the correct Pb-loading of $1/7 \rightarrow 1/8$ substitution of Bi will require 50% of the eligible Bi(1) and Bi(4) sites to be substituted, and will give a periodic structure $7 \times a/2$, $7 \times a/2$, $6 \times a/2$, with an average superspacing of $A_2 = 6.67 \times a/2$. This substitution is shown schematically in Fig. 10(*a*), where the lateral stacking sequence is shown in terms of the Bi-atom labels 1–5 used by Le Page *et al.* (1989). Bearing in mind that a required spacing is $\sim 7 \times a/2$ for the basic modulation (our experimental results), we can accommodate this by reducing the size of two out of every three primary supercells from $A_1 = 5 \times a$ to $A_1 = 4.5 \times a$, corresponding to 9 instead of 10 Bi atoms along x. This same change will then bring the average value of A_1 down from 5 to the incommensurate value of $4.67 \times a$, *i.e.* within experimental accuracy of the measured value of $4.7 \times a$.

This final model is shown in Fig. 10(*b*) where both the q_1 spacing (varying between 9 and 10 structural subunits) and the equivalent q_2 spacing are shown, above and below the ordering sequence respectively. At this stage we have satisified the three constraints imposed by the data *i.e.* by satisfying the first two constraints of a definite q_2 value and a measured Pb content we have incidently satisfied the third.

The substitutional structures of Fig. 9 in conjunction with the modelling above also allows many observed diffraction features to be interpreted. For example, incorporation of both Pb^{2+} and Pb^{4+} at both expanded and compressed zones of the Bi—O layer, *i.e.* at both nodes and antinodes of the centering in the Q_1 structure (see space-group discussion below) would explain the lack of corresponding centering in the Pb-based superlattice. Statistical occupation of the B(1) sites would contribute to the diffuse streaks observed along ⟨110⟩ directions (Fig. 1*c*); this model (Fig. 9*c*) would also satisfactorily explain the preponderance of the $(Q_1 - Q_2)$ vector found in the patterns.

One advantage of this argument is that it allows an explanation of differing observed symmetries (*Amaa* and *A2aa*) in terms of ordering. From Fig. 9(*d*) it is seen that if a superstructure is built in a certain way there can be symmetrical units (as for example with the repeat sequence: 10–10–9–10–10–9–

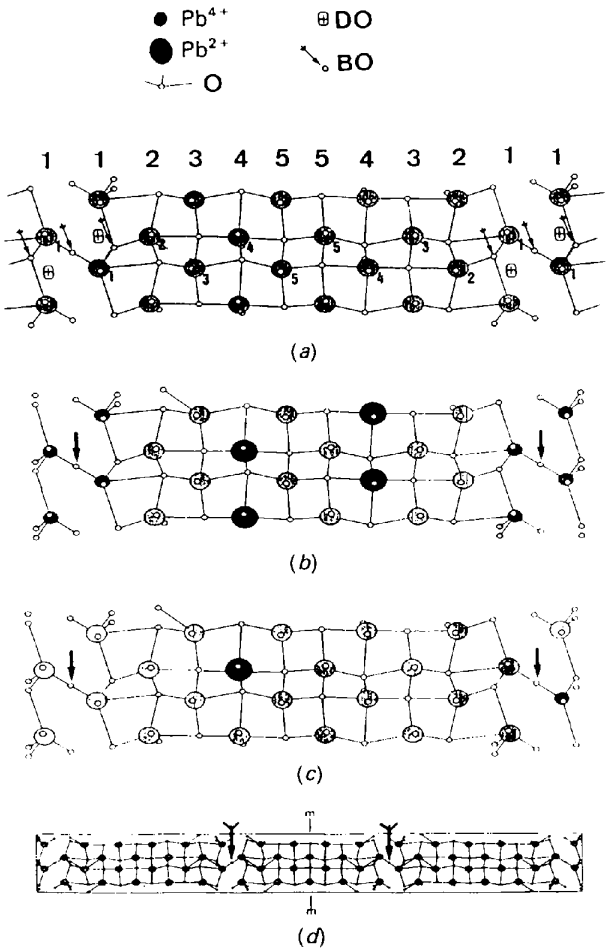

Fig. 9. (*a*) Topology of a Bi—O layer in $Bi_{10}Sr_{15}Fe_{10}O_{36}$ following Le Page *et al.* (1989), with labels 1–5 for the five distinct Bi-atom coordination sites, following the nomenclature of these authors. Oxygen shifts are indicated by the symbols, as: DO = (2) displaced O atoms (from the rock-salt position). BO = (3) bridging O positions. (*b*) The same layer, showing a statistical averaged occupation of Bi(1) and Bi(4) sites by Pb^{4+} and Pb^{2+} ions respectively. (*c*) The same layer, with occupation of Bi sites by Pb^{4+} and Pb^{2+} at distances required by the present model (only one Bi—O string is shown with Pb replacement). (*d*) A string of three supercell units of 10–9–10 half-unit-cell lengths, showing a centrosymmetric unit.

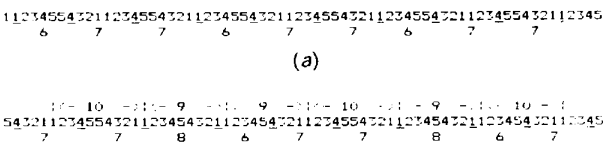

Fig. 10. Sequence of Bi-atom types, using the numbering 1–5 of Le Page *et al.* (1989), forming a semi-random sequence: (*a*) The regular sequence incorporating Pb in 50% of Bi(1) and Bi(4) sites. The substituted sites are underlined; the length of superperiod between substituted sites is given in units of $a/2$, below each supercell. (*b*) Final model, in which alternate sequences of primary superperiods of lengths $5a$ and $4.5a$ occur in semi-random fashion. The lengths of superperiods between bridging oxygens are given above the sequence, in units of $a/2$ multiples, while the corresponding lengths of Pb-site superperiods are given in the same units below the sequence.

9–9–10–10 *etc.*, as contrasted with the sequence 10–10–9–9–10–10–), involving a symmetry induced by twinning of the asymmetric bridging oxygen sites. Therefore it is possible for the property of centrosymmetry to be determined by specific lateral ordering, the space group then becoming sensitive to details of preparation. Alternatively (or equivalently), the higher symmetry can be interpreted as arising out of a systematic micro-twinning between noncentrosymmetric units, on a sufficiently fine scale.

5.2. *Symmetry expansion to the* 2212 *structure*

In order to relate the ferrite structure to that of the 2212 phase the space group *B*222 needs to be expanded to that of *N.A2aa*.111. The main task in this extension is the modification of the stretching mode parallel to '*a*' to be anti-phase along '*b*' in keeping with the *a* glide of *A*2*aa*. This mode was described quantitatively by Gao, Lee, Coppens, Subramanian & Sleight (1988). Maintaining consistency with their values, this modification is achieved in Fig. 11(*a*), where the additional oxygen acts to alternatively expand and contract neighbouring rows in the '*b*' direction. Further expansion, introducing the *I* centering (responsible for the $L + K + m = 2n$ rule for *N.A*2*aa*.111) is achieved schematically in Fig. 11(*b*), showing two of the four Bi—O layers of the structure. The fact that the covering three-dimensional group for this structure is *I*222, and that this is the only space group which would be evident if the modulation was regular and gave rise to strong reflections, serves to illustrate the value of superspace descriptions which permit all the observable symmetries to be incorporated.

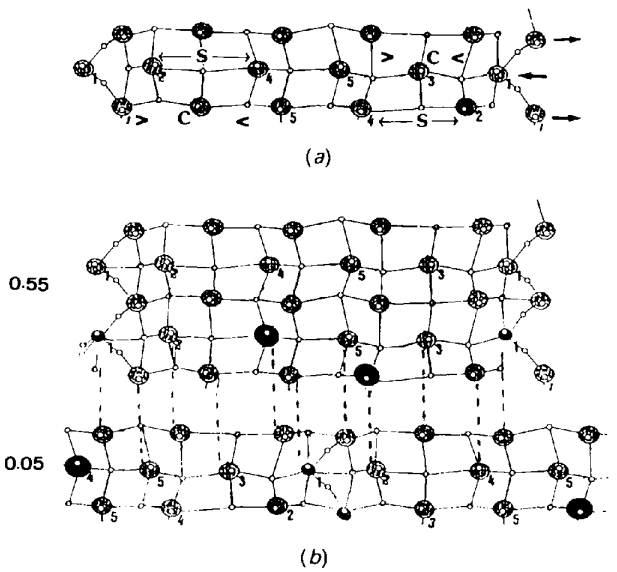

Fig. 11. (*a*) Model for single Bi—O layer with a commensurate fivefold superlattice following Le Page *et al.* (1989), with *a*-glide symmetry relating the alternate stretched (S) and compressed (C) zones induced by the bridging oxygens, following the work of Gao *et al.* (1988). (Note: positional phases of these authors are followed, with an increased amplitude for diagramatic illustration.) (*b*) Extension of the model to include the *I* centering of *I*222, showing two of the four Bi—O layers, at $z = 0.55c$ and $0.05c$, with some Pb-atom replacements. Note that the lattice stretching mode is in phase for these layers in [001] projection, consistent with *N.A*2*aa*.111 symmetry observations. (Note: displacements parallel to '*c*', important in [010] projection, are not shown here.) The atom code for Pb^{4+}, Pb^{2+} is the same as for Fig. 9.

6. Summary and concluding remarks

Our present CBED observations, like those of Kan *et al.* (1990), are consistent with the non-centrosymmetric space group *A*2*aa* for the 2212 parent structure. The asymmetry of the patterns is such that the *cations* must be moved off centrosymmetric positions in the average structure. Thus simple O-atom shifts as suggested earlier by Bordet, Capponi, Chaillot, Chanavas, Hewat, Hewat, Hodeau, Marezio, Tholence & Tranqui (1988) would not suffice, but the later finding from X-ray single-crystal analysis by Petricek *et al.* (1990) that both Bi and O atoms are located on noncentrosymmetric sites within *A*2*aa* is more consistent with our results.

Our present analysis in terms of order–disorder with particular Bi-site doping by Pb gives an explanation of the main observations so far made on the 2212 structure $Pb_xBi_{2-x}Sr_2CaCu_2O_{6+\delta}$ with $x = 0.23$, where the two (q_1 and q_2) superstructures coexist. In a publication received after our first submission, Hirotsu, Ikeda, Ichinose, Nagakura, Komatsu & Matsushita (1991) present direct evidence for the random sequencing of 9 and 10 half-unit-cell blocks in this particular compositional regime. This agreement with direct high-resolution imaging provides a timely illustration of the complementary nature of present diffraction and real-space methods. For example there is a divergence of interpretation with respect to symmetry. Whereas the above authors place emphasis on a transition from tetragonal to orthorhombic symmetry as basic to changes in the superstructure, CBED evidence of the tetragonal phase is lacking; our evidence suggests that there is no tetragonal phase, even when $a = b$, $\gamma = 90°$ as for the 2223 structure (not examined here), and that the superlattice and parent-structure symmetry are not so simply related.

Finally, the detection of a 'swinging' crystallographic shear plane (CS) structure in some of the diffraction patterns means that at best, the model of Pb substitution within a single incommensurate structure is an averaged description, for a particular composition. More generally, the incommensurate lattice itself is immersed in a low-angle shear struc-

ture yet to be given a detailed description. However, the CS mechanism would normally play a significant role in accounting for a variable oxygen loading, and the additional compositional flexibility which this mechanism allows could well account for the spread in both symmetry allocation and in superconducting properties reported for these compounds.

The collaboration of the Monash Physics School in providing crystals from Pb-free 2212 compound is gratefully acknowledged. We are also grateful to the Australian Research Council for supporting this project (grant A68930390). Finally we wish to acknowledge assistance given to us by Shaun Bulcock in exploring various preparative paths, and in computing the content for Fig. 9.

References

BOEKHOLT, M., GÖTZ, D., IDINK, H., FLEUSTER, M., HAHN, T., WOERMANN, E. & GUNTHERODT, G. (1991). *Physica C*, **176**, 420–428.

BORDET, P., CAPPONI, J. J., CHAILLOUT, C., CHENAVAS, J., HEWAT, A. W., HEWAT, E. A., HODEAU, J. L., MAREZIO, M., THOLENCE, J. L. & TRANQUI, D. (1988). *Physica C*, **156**, 189–192.

BURSILL, L. A. & HYDE, B. G. (1972). *Prog. Solid State Chem.* **7**, 178–220.

CHEN, C. H., WERDER, D. J., ESPINOSA, G. P. & COOPER, A. S. (1989). *Phys. Rev. B*, **39**, 4686–4689.

FUNG, K. K., YANG, C. Y. & YAN, Y. F. (1989). *Appl. Phys. Lett.* **55**, 280–282.

GAO, Y., LEE, P., COPPENS, P., SUBRAMANIAN, M. A. & SLEIGHT, A. W. (1988). *Science*, **241**, 954–956.

GOODMAN, P. (1975). *Acta Cryst.* A**31**, 804–810.

HIROTSU, Y., IKEDA, Y., ICHINOSE, Y., NAGAKURA, S., KOMATSU, T. & MATSUSHITA, K. (1991). *Electron Microsc.* **40**, 147–156.

JOHNSON, A. W. S. (1972). *Acta Cryst.* A**28**, 89–91.

KAN, X. B., KULIK, J., CHOW, P. C. & MOSS, S. C. (1990). *J. Mater. Res.* **5**, 731–736.

LE PAGE, Y., MCKINNON, W. R., TARASCON, J. M. & BARBOUX, P. (1989). *Phys. Rev. B*, **40**, 6810–6816.

MAEDA, H., TANAKA, Y., FUKUTOMI, M. & ASANO, T. (1988). *Jpn. J. Appl. Phys.* **27**, 209.

PETRICEK, V., GAO, Y., LEE, P. & COPPENS, P. (1990). *Phys. Rev. B*, **42**, 387–392.

RAMESH, R., VAN TENDERLOO, G., THOMAS, G., GREEN, S. M. & LUO, H. L. (1988). *Appl. Phys. Lett.* **53**, 2220–2222.

SEQUEIRA, A., RAJAGOPAL, H., SASTRY, P. V. P. S. S., YAKHMI, J. V. & IYER, R. M. (1991). *Physica C*, **173**, 267–273.

TANAKA, M., TERAUCHI, M. & KANEYMA, T. (1988). *Convergent-Beam Electron Diffraction*, Vol. II. Tokyo: Jeol Ltd.

TARASCON, J. M., LE PAGE, Y., BARBOUX, P., BAGLEY, B. G., GREENE, L. H., MCKINNON, W. R., HULL, G. W., GIROUD, M. & HWANG, D. M. (1988). *Phys Rev. B*, **37**, 9382–9389.

WEN, J. G., LIU, Y., REN, Z. F., YAN, Y. F., ZHOU, Y. Q. & FUNG, K. K. (1989). *Appl. Phys. Lett.* **55**, 2775–2777.

WITHERS, R. L., ANDERSON, J. S., HYDE, B. G., THOMSON, J. G., WALLENBERG, L. R., FITZGERALD, J. D. & STEWART, A. M. (1988). *J. Phys. C*, **21**, L417–L424.

WOLFF, P. M. DE, JANSSEN, T. & JANNER, A. (1981). *Acta Cryst.* A**37**, 625–636.

YAMAMOTO, A. (1991). *Phys. Rev. B*. Submitted.

YAMAMOTO, N., HIROTSU, Y., NAKAMURA, Y. & NAGAKURA, S. (1989). *Jpn. J. Appl. Phys.* **28**, L598–L601.

ZHANG, X. F., YAN, Y. F. & FUNG, K. K. (1990). *Mod. Phys. Lett.* **B4**, 605–611.

Acta Cryst. (1992). B**48**, 389–392

$LaNi_2Al_3$, a Ternary Substitution Variant of the Orthorhombic $BaZn_5$ Type

BY R. E. GLADYSHEVSKII, K. CENZUAL AND E. PARTHÉ

Laboratoire de Cristallographie aux Rayons X, Université de Genève, 24 Quai Ernest-Ansermet, CH-1211 Geneva 4, Switzerland

(*Received* 1 *July* 1991; *accepted* 3 *February* 1992)

Abstract

Lanthanum dinickel trialuminide, $LaNi_2Al_3$, M_r = 337.28, orthorhombic, *oS*24, *Cmcm–gec*^{2} (No. 63), a = 10.173 (1), b = 7.834 (1), c = 5.1374 (7) Å, V = 409.43 (9) Å^3, Z = 4, D_x = 5.471 mg mm^{-3}, λ(Mo $K\alpha$) = 0.71073 Å, μ = 19.904 mm^{-1}, F(000) = 608, T = 293 K, R = 0.039, wR = 0.034 for 318 contributing unique reflections. The structure is a ternary ordered variant of the $BaZn_5$ type. As in the two other structure types reported for RNi_2Al_3 compounds (R = rare-earth metal), *i.e.* the hexagonal YNi_2Al_3 and $PrNi_2Al_3$ types, Kagome nets are found. In $LaNi_2Al_3$ these nets are strongly distorted and are formed exclusively by Al atoms. The Ni atoms are located between the Kagome nets and the La atoms inside the nets. The $LaNi_2Al_3$ and $BaZn_5$ types can further be considered as vacancy variants of Pu_3Pd_5 which crystallizes in the same space group.

Introduction

Six compounds were reported for the La–Ni–Al system by Bodak & Gladyshevskii (1985). Structure types are known for two of these, *i.e.* $LaNi_{5\rightarrow4}Al_{8\rightarrow9}$ with $NaZn_{13}$ type and $LaNi_2Al_5$ (Yarmolyuk, Rykhal', Aksel'rud & Zarechnyuk, 1981) with

0108-7681/92/040389-04$06.00